LUBRICATION SCIENCE
Lubrication Science 2017; **29**:183–199
Published online 10 November 2016 in Wiley Online Library (wileyonlinelibrary.com). DOI: 10.1002/ls.1363

Optimising the design of textured surfaces for reducing lubricated friction coefficient

Javier Echávarri Otero*,†, Eduardo de la Guerra Ochoa, Irene Bellón Vallinot and Enrique Chacón Tanarro

Grupo de Investigación en Ingeniería de Máquinas, Universidad Politécnica de Madrid, Madrid, Spain

ABSTRACT

Under operating conditions which are unfavourable for lubrication, such as high load and low velocity, the use of textured surfaces significantly promotes the formation of a thick lubricant film and an improvement of the friction coefficient. This paper relates to the manufacture of textures using a photolithography and chemical etching process. Different surface geometries, texturing densities and depths were designed to analyse the influence of these parameters. The friction coefficient was measured in a ball-on-disc tribometer under different lubrication regimes, and the results have been used to develop an artificial neural network with texturing optimisation potential. © 2016 The Authors *Lubrication Science* published by John Wiley & Sons Ltd.

Received 9 May 2016; Revised 16 September 2016; Accepted 9 October 2016

KEY WORDS: friction coefficient; surface texturing; photolithography; point contact; artificial neural network

INTRODUCTION

Many lubricated systems can end up operating under mixed and boundary regimes, especially in contacts at high loads or low velocities. This is the case of point and line contacts in machines, such as those that occur in bearings or gears. Under these conditions, friction can be reduced by modifying the properties of the lubricant, as multiple references published in the past few decades show.[1–4]

The complexity of these studies is increased because of the usually limited knowledge about the behaviour of the lubricant under high pressure and high shear rate conditions typical of point and line contacts.[5] This means that it is very difficult to accurately predict the thickness of the lubricant film[5,6] and the potential existence of direct contacts between the lubricated surfaces.

In addition to the actions on the lubricant, many studies have been recently conducted on the improvement of friction through the surface geometry of the bodies in contact, which includes the surface finish, the coatings and the surface texturing.[7–11] The present paper studies different types of textures to find out which ones decrease the friction coefficient the most.

*Correspondence to: Javier Echávarri Otero, Grupo de Investigación en Ingeniería de Máquinas, Universidad Politécnica de Madrid, Madrid, Spain.
†E-mail: jechavarri@etsii.upm.es

More specifically, we analyse the textures based on small dimples acting as lubricant reservoirs,[12,13] which play an important role under demanding lubrication conditions and facilitate the existence of a fluid film separating both surfaces. Based on the thickness of the lubricant film h and the roughness of the surfaces (σ_1 and σ_2), the specific film thickness[14] is defined as follows:

$$\lambda = \frac{h}{\sqrt{\sigma_1^2 + \sigma_2^2}} \tag{1}$$

The values of this parameter allow the boundary, mixed and fluid film lubrication regimes to be characterised,[15] as shown in Table I. These regimes are depicted in the Stribeck curve (Figure 1), which represents the variation of the friction coefficient with regard to the specific film thickness.

As Figure 1 shows, surface texturing modifies the curve and enlarges the fluid film lubrication regime. Thus, the additive load and viscosity requirements of the lubricant can be reduced, while achieving sufficient film thickness to keep friction low. In addition, the lubricant enters the dimples and produces a local hydrodynamic wedge effect.[16–18] Another function of surface textures is that of trapping detached metal particles and impurities in general.[12,13,17] This may contribute to the lubricant retaining its properties for a longer time, which results in a greater tribological care of the system.

According to the references[16,19–25], the parameters which are deemed to have a greater influence during the design of textured patterns are surface geometry (texture shape, orientation and size), depth and texturing density. However, these are not the only parameters which influence the final behaviour of the contact since, e.g. the texturing method may affect the final quality.[26]

The references show tests with textures having a great variety of shapes, the most widely developed being that based on circular dimples, as it achieves greater friction coefficient reductions than triangular or linear patterns.[16,20] However, several authors point out the benefits of elliptical geometries, being

Table I. Lubrication regimes as a function of λ.

Boundary lubrication	$\lambda < 1$
Mixed lubrication	$1 < \lambda < 3$
Fluid film lubrication	$\lambda > 3$

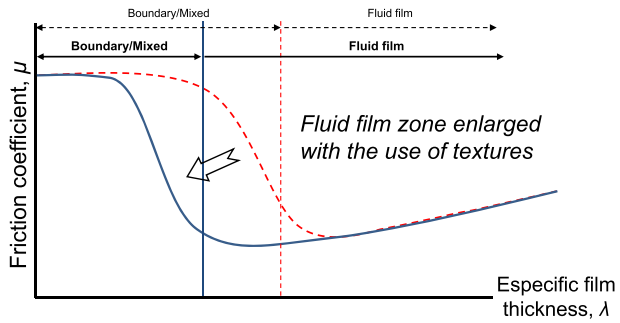

Figure 1. Modification of the Stribeck curve with the use of textures. [Colour figure can be viewed at wileyonlinelibrary.com]

DOI: 10.1002/ls

the orientation of ellipses with regard to the direction of sliding another parameter of influence.[17] In accordance with these references, elliptical textures whose major axis is perpendicular to the direction of sliding attain a maximum reduction of the friction coefficient. A commonly employed ratio is 1×4, i.e. a major axis of the ellipse four times longer than the minor axis.

As far as size is concerned, Wakuda *et al.*[19] show that for the case of circular patterns, the optimal size of these textures is related to the Hertzian contact width. Consequently, this parameter is closely related to the operating conditions since the load value has a great influence on contact width.

The texturing density, defined as the ratio of the area covered by the textures to the total surface area, is considered to be a parameter which is less influential on friction than others.[27] Several studies disclose that the optimal value is between 5% and 20%[19,21,23,28] and is very often lower than 10%.

Finally, depth is a parameter that is difficult to control and measure, which is why there are just a few previous studies about it. The existing references[19–22,25] focus on specific applications, so their scope is limited, and it is difficult to draw any general conclusions from them. They include tests with textures of depths ranging from 3.2 to 380 µm.

TEXTURING THE SURFACES

The textures were created on a flat side of copper discs so as to subsequently test the point contact between a steel ball and the discs in a tribometer under 5 and 20 N loads, which correspond to the test conditions used in earlier studies.[28]

There are many techniques for removing material on metal surfaces in a controlled manner.[26,27] The photolithography and chemical etching process has been chosen due to its simplicity and the efficacy shown in previous analyses.[28] The photolithographic equipment used was the SF-100 from Intelligent Micro Patterning (www.intelligentmp.com), which is shown in Figure 2. The same figure depicts the Olympus DSX 500 high-resolution opto-digital microscope (www.olympus-ims.com), which was used to make a final inspection on the texturing.

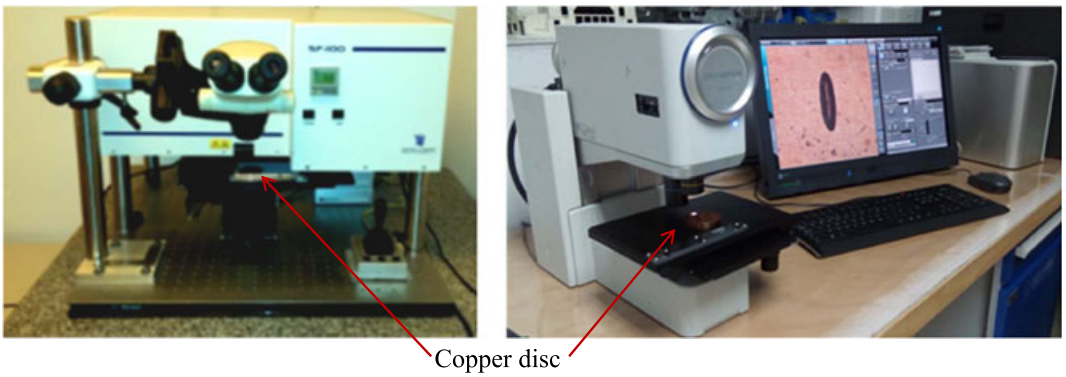

Figure 2. Intelligent Micro Patterning SF-100 and Olympus DSX 500. [Colour figure can be viewed at wileyonlinelibrary.com]

DOI: 10.1002/ls

Stages of the process

The first stage consists in placing a photoresist (a light-sensitive film) on the surface which is going to be textured by means of the application of heat and pressure (Figure 3a). The other parts of the specimen are protected.

Once each test specimen has been prepared, the photoresist is exposed to monochromatic ultraviolet light in the SF-100 by using different virtual masks (Figure 3b) generated by means of a computer-aided design programme. Each mask contains two colours: white, where the photoresist hardens during exposure and stays on the test specimen to protect it during the subsequent etching, and black, which does not cure and is subsequently removed. To eliminate uncured areas, the photoresist layer is subjected to a development in a Na_2CO_3 bath (0.85 wt% in H_2O). Thus, the photoresist only remains adhered to those parts of the surface of the test specimen which are not to be textured, as shown in Figure 3c.

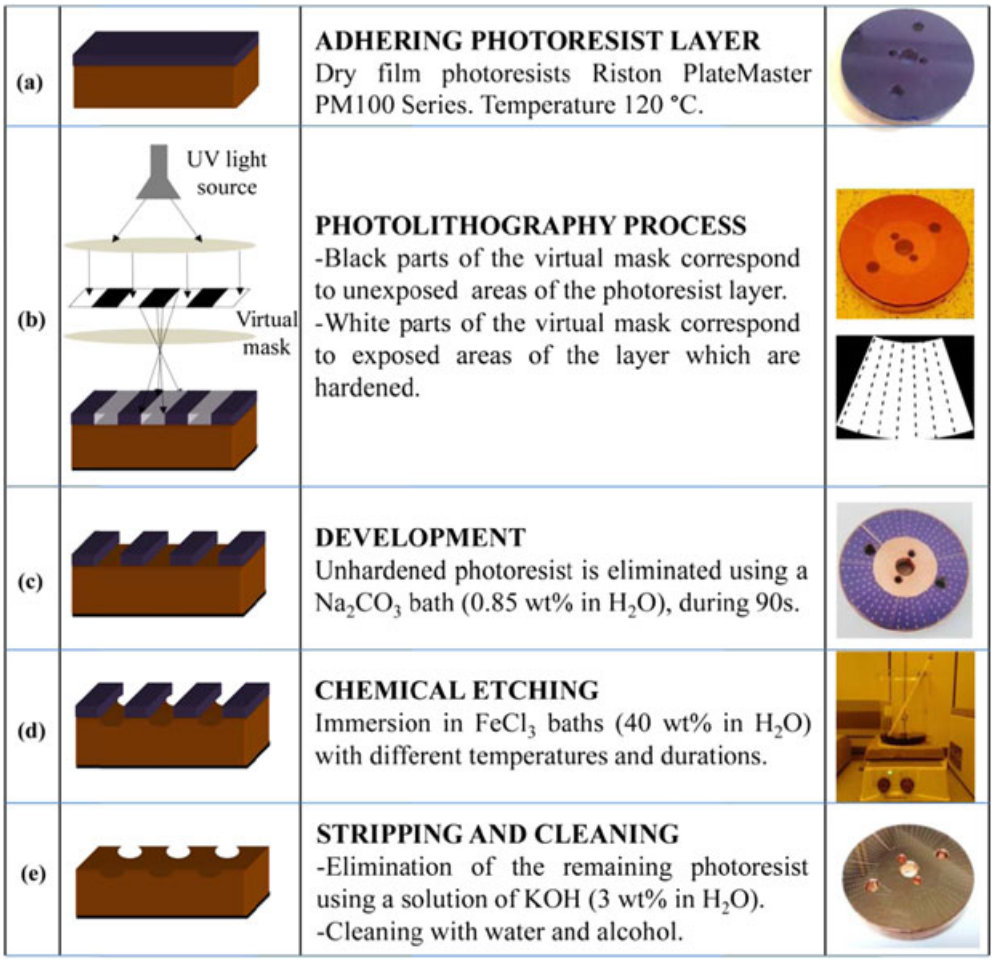

Figure 3. Outline of photolithography and chemical etching process. [Colour figure can be viewed at wileyonlinelibrary.com]

DOI: 10.1002/ls

Textures are created by chemical etching, for which the test specimen is submerged in a $FeCl_3$ bath (40 wt% in H_2O), as shown in Figure 3d. The temperature and time of said bath determine the depth of the texture generated during etching. Subsequently, the protective photoresist is stripped, i.e. completely removed, from the test specimen by putting it in a KOH bath (3 wt% in H_2O), as shown in Figure 3e. Finally, the test specimen is thoroughly cleaned with water and alcohol and protected until it is tested.

Manufactured textures

As already mentioned, copper discs were selected to apply the photolithography and chemical etching process. The use of a homogeneous base material like copper lets us achieve a very uniform surface texturing after the chemical etching process. In contrast, etching other materials like steel leads to more heterogeneous texture shapes and depths. Therefore, the copper specimens provide more reliable and repeatable results when creating textures by chemical etching.

As stated earlier, the influencing parameters which were taken into account during the design of the patterns were surface geometry (shape, orientation and size), depth and surface density.

An elliptical geometry was chosen for the textures, the major axis being orientated perpendicular to the sliding direction, in line with the results of previous works.[12,16] In addition to the 1×4 ratio used in several references[23,24], textures based on 1×2 and 1×6 ellipses were also created to analyse their effect on the friction coefficient.

The size was selected based on the half-width of the Hertzian contact a, which was calculated by using the Equations 2 for the point contact, where W is the normal load, R is the radius of the ball, E' is the reduced Young's modulus and p_0 is the maximum Hertzian pressure.[29]

$$p_0 = \frac{3W}{2\pi a^2} \qquad a = \sqrt[3]{\frac{3WR}{2E'}} \qquad \frac{2}{E'} = \frac{1-\upsilon_1^2}{E_1} + \frac{1-\upsilon_2^2}{E_2} \tag{2}$$

E_1, E_2 being the Young's moduli of the materials in contact and υ_1, υ_2 the respective Poisson's ratios. Table II shows the properties of the materials used, which lead to steel–copper contact widths of 150 and 240 μm according to Equation 2 for loads of 5 and 20 N respectively.

Bearing in mind the previously mentioned influence of the texture size on the results, minor axis sizes similar or larger than the Hertzian contact width were chosen for the case of the 5 N load, whereas in the case of the 20 N load, sizes smaller and larger than Hertzian width were selected. Specifically, patterns were created by using 150×300, 150×600, 150×900 and 250×1000μm ellipses.

The surface density ranged from 5 to 10%, according to the information available in prior works.[19,21,23,28] Likewise, different combinations of time (8–20 min) and chemical etching temperatures (25–40°C) were used, which allowed — in the absence of conclusive prior studies on depth — a sufficient wide range to be obtained for analysis: 17, 35 and 78 μm.

Table II. Properties of the materials.

Specimen	Material	E(GPa)	υ	R(mm)
Ball	Steel E-52100	210	0.30	9.525
Disc	Copper	117	0.34	∞

DOI: 10.1002/ls

Table III summarises the range of the texturing parameters studied, whose combinations were used to analyse the influence of the design of surface texturing on the friction coefficient by comparing the results to untextured specimens.

Once the textured discs were created, the surface geometry, texturing density and depth were inspected under the high-resolution microscope DSX 500. Figure 4 shows some results of images at different scales, which have enabled us to verify that the dimensions match the intended ones, without significant deviations.

FRICTION TESTING IN TRIBOMETER

Tribological test equipment

The tribological equipment used to test the textured discs was the Mini Traction Machine (MTM) from PCS Instruments (www.pcs-instruments.com), which is shown in Figure 5. It measures the friction coefficient on lubricated point contacts under a wide range of rolling and sliding conditions. The following parameters can be controlled: the temperature of the lubricant bath, the normal load W,

Table III. Range of texturing parameters created.

Size (μm)	150 × 300, 150 × 600, 150 × 900 and 250 × 1000
Density (%)	5 and 10
Depth (μm)	17, 35 and 78

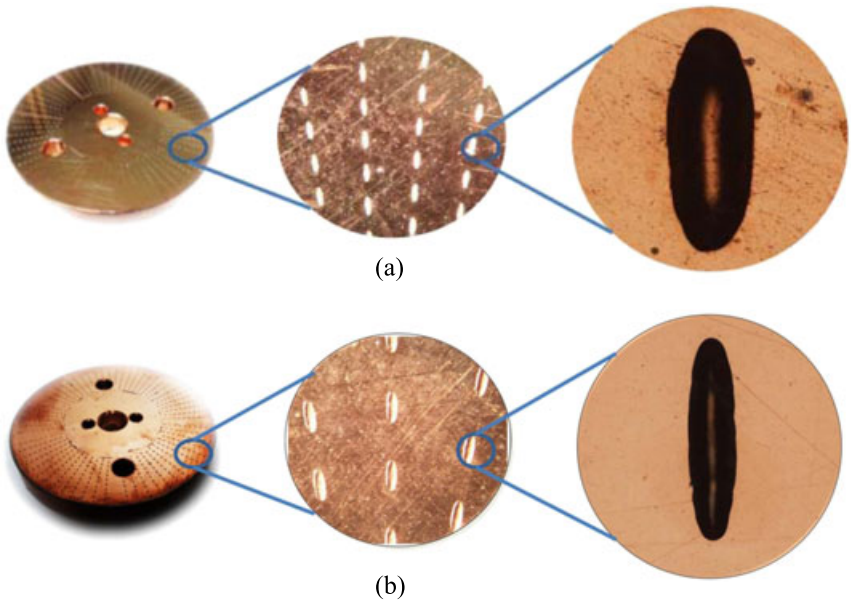

Figure 4. Examples of textures created: different scale views. (a) Ellipses 150 × 600 μm, texturing density 10% and depth 78 μm. (b) Ellipses 150 × 900 μm, texturing density 5% and depth 78 μm. [Colour figure can be viewed at wileyonlinelibrary.com]

DOI: 10.1002/ls

Figure 5. Mini Traction Machine. Overview and detail of the ball-on-disc contact. [Colour figure can be viewed at wileyonlinelibrary.com]

the average velocity u_m and the slide-to-roll ratio (SRR), defined in Equation 3, where Δu is the sliding velocity.

$$\mathrm{SRR}(\%) = \frac{\Delta u}{u_m} 100 \tag{3}$$

The MTM works under all lubrication regimes, from fluid film to mixed and boundary lubrication; the latter two are the most important for this paper since a greater influence of the texturing on friction is expected to take place in them, as shown in Figure 1.

In order to facilitate a comparison of the new results to those obtained previously, the materials chosen and the conditions selected for tests in the MTM tribometer were those used in earlier studies[28], i.e. normal loads of 5 and 20 N (equivalent to Hertzian pressures of 0.42 and 0.67 GPa respectively), PAO-6 lubricant at a constant bath temperature of 40°C, average velocities ranged from 100 to 3500 mm s^{-1} and SRRs ranged from 5 to 100%.

To perform approximate estimations of film thickness, the dynamic viscosity at atmospheric pressure η_0 and the viscosity-pressure coefficient α for this lubricant can be taken from reference[30]. The values at 40°C are $\eta_0 = 25$ mPa · s and $\alpha = 11.5$ GPa^{-1}. The balls and discs used in the tests were highly polished, and their surface roughness (RMS) was 12 and 24 nm respectively.

Figure 6a shows the location of the test conditions on the Hamrock-Dowson chart, based on the viscosity parameter g_V and the elasticity parameter g_E[30] shown in Equation 4. They correspond to the most general case: pressure-dependant viscosity (piezoviscosity) and existence of elastic deformation. Under these conditions, the classic Hamrock and Dowson formula[6] can be applied to roughly estimate the central film thickness by means of Equation 5.

$$g_V = \frac{\alpha W^3}{(\eta_0 u_m)^2 R^4} \qquad g_E = \frac{W^{8/3}}{(\eta_0 u_m)^2 E'^{2/3} R^{10/3}} \tag{4}$$

DOI: 10.1002/ls

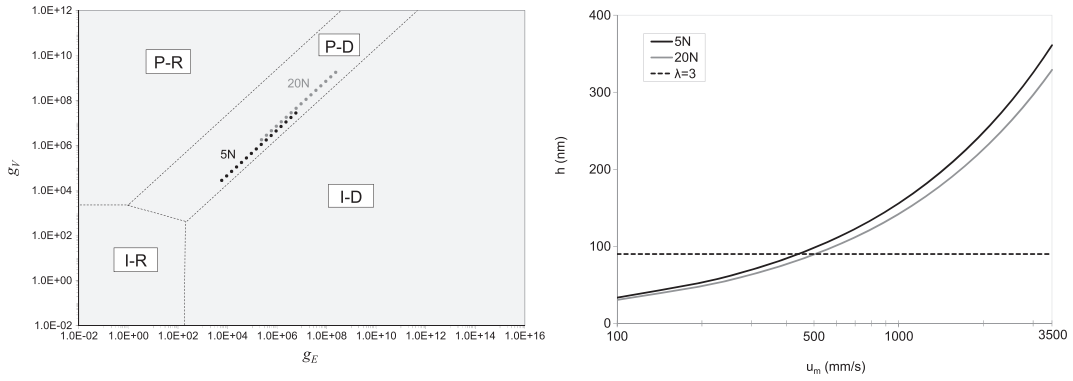

(a) (b)

Figure 6. (a) Location of the test conditions in the Hamrock–Dowson chart (I-R: Isoviscous/Rigid, I-D: Isoviscous/elastic-Deformation, P-R: Piezoviscous/Rigid, P-D: Piezoviscous/elastic Deformation). (b) Distinction between lubrication regimes according to specific film thickness.

$$h = 1.55\alpha^{0.53}(\eta_0 u_m)^{0.67} E'^{0.061} R^{0.33} p_0^{-0.201} \tag{5}$$

The specific film thickness results are shown in Figure 6b. Different lubrication regimes are expected in the tests, bearing in mind that the combined surface roughness of the specimens is smaller than 30 nm. In this way, we can analyse the effect of the textures both under fluid film ($\lambda > 3$) and boundary/mixed ($\lambda < 3$) conditions.

TEST RESULTS

The textured discs were tested in the MTM to obtain the friction coefficient under different operating conditions. Over 1000 experimental records were obtained, which enabled us to assess the developed texture designs.

Relevant graphs obtained experimentally are shown in Figures 7 to 11. They show the expected shape according to the lubrication regimes of the Stribeck curve. The results have been depicted in all figures versus an untextured disc and show that surface texturing is an effective alternative for reducing the friction coefficient in point contacts, particularly at low velocities and high pressures, which lead to boundary/mixed lubrication conditions.

Figure 7 shows the differences between the different surface geometries for a 5% density and 78 μm depth in a test at 20 N and SRR = 50%. It can be seen in this case how the trend towards very eccentric ellipses provides an almost negligible friction improvement. Nevertheless, 150 × 600 μm ellipses, i.e. those with a 1 × 4 ratio between the minor and the major axes, are the ones that cause a greater reduction of the friction coefficient.

The graph of Figure 8a compares tests conducted under two loads on surfaces textured with 150 × 600 μm ellipses. A reduction of similar magnitude is observed at 5 and 20 N for boundary/mixed conditions, whereas under fluid film lubrication, the curves for textured and

DOI: 10.1002/ls

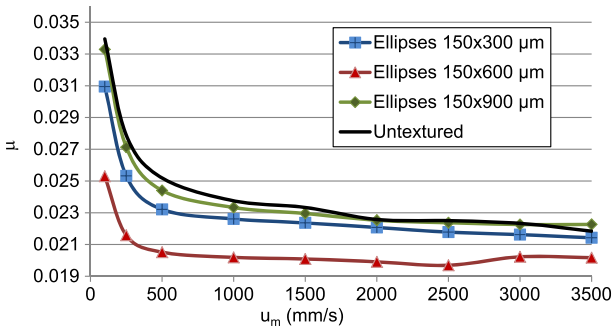

Figure 7. Influence of surface geometry on friction coefficient. $W = 20$ N, SRR = 50%, texturing density 5%, depth 78 μm. [Colour figure can be viewed at wileyonlinelibrary.com]

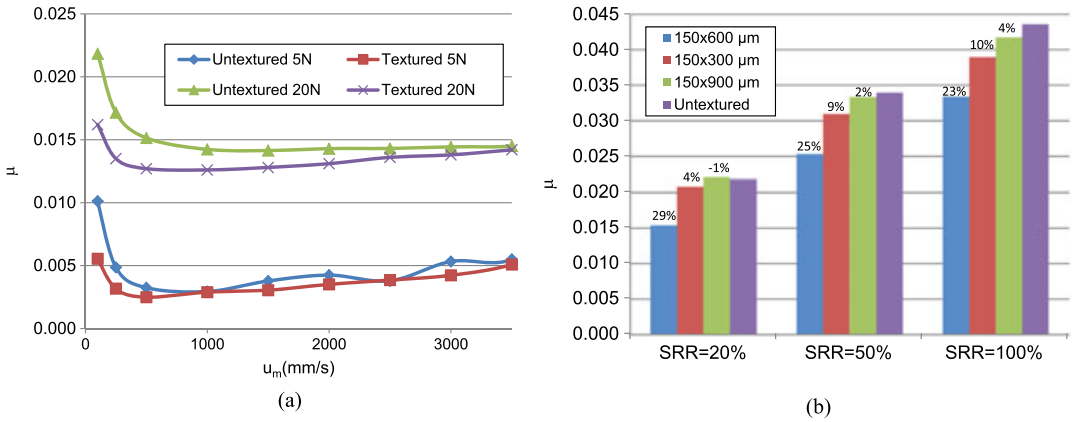

Figure 8. (a) Load effect on friction coefficient. SRR = 20%, ellipses 150 × 600 μm, texturing density 5%, depth 35 μm; (b) SRR effect on friction coefficient: percentage reduction with respect to untextured specimens. Ellipses 150 × 600 μm, $W = 20$ N, $u_m = 100$ mm s^{-1}, texturing density 5% and depth 78 μm. [Colour figure can be viewed at wileyonlinelibrary.com]

untextured specimens come closer together, especially at 5 N. From a practical point of view, this is an advantage since it means that the texturing is effective for different loads under boundary/mixed regime, regardless of the reference value used for load when designing the texture. Likewise, Figure 8b shows the results for different SRRs and average velocity of 100 mm s^{-1}, which corroborate the friction behaviours observed in Figure 7 for SRR = 50%. Consequently, in the successive analyses, results are compared at 20 N and SRR = 50%.

As observed in Figure 8b, there is a slight variation of the percentage reduction of friction coefficient with the SRR, e.g. between 23% and 29% for the elliptical geometry 150 × 600 μm. The results show a more stable trend than those obtained previously for circular geometries.[19,28] Despite the depths of the circular and elliptical dimples are slightly different, a preliminary comparison shows a better behaviour of elliptical textures for higher SRR.

DOI: 10.1002/ls

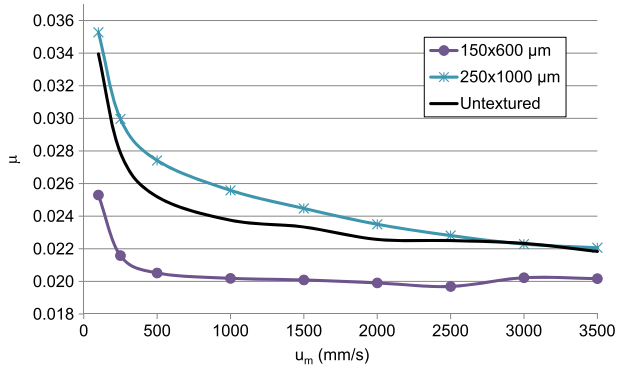

Figure 9. Influence of size on friction coefficient. $W = 20$ N, SRR = 50%, texturing density 5% and depth 78 μm. [Colour figure can be viewed at wileyonlinelibrary.com]

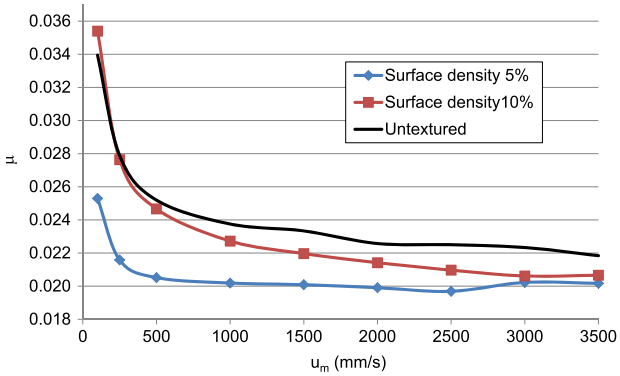

Figure 10. Influence of texturing density on friction coefficient. $W = 20$ N, SRR = 50%, ellipses 150 × 600 μm and depth 78 μm. [Colour figure can be viewed at wileyonlinelibrary.com]

In regards to size, Figure 9 shows the results for two designs tested against an untextured disc, for a 1 × 4 ratio between axes, a 78 μm depth and a 5% density. The results indicate that the 150 × 600 μm size brings about a clear reduction of the friction coefficient, which for a 20 N load corresponds to the case of the minor axis being smaller than the Hertzian contact width. This result confirms the dependence of the friction coefficient on the size of the pattern, as stated in several references[19,28] for the case of the surfaces textured with circular geometries. Our tests for elliptical geometries indicate that the use of minor axes of a size smaller than the contact width leads to a greater reduction of the friction coefficient, in line with the results obtained by the authors for circular geometries.[28]

A higher density would apparently lead to an increase in lubricant reservoirs and, hence, a better behaviour against friction, but this influence is a lot more complex because the flow lines described by the lubricant are modified.[23] Figure 10 shows that a density of 5% yields better results than higher densities, thus corroborating the conclusions of references[19,23,28] for other geometries.

If the friction results obtained for the three depths tested are compared, Figure 11 shows that the disc with the greatest texturing depth (78 μm) leads to a greater decrease of the friction coefficient with

DOI: 10.1002/ls

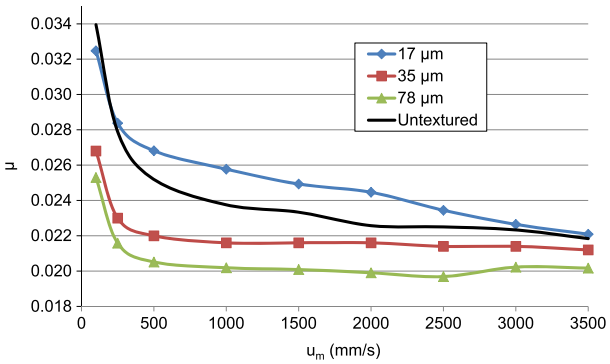

Figure 11. Influence of depth on friction coefficient. $W = 20$ N, SRR = 50%, ellipses 150 × 600 μm and texturing density 5%. [Colour figure can be viewed at wileyonlinelibrary.com]

regard to the untextured specimen. However, texturing to a very low depth does not show any beneficial effects with regard to the untextured surface.

Table IV shows the maximum percentage reduction of the friction coefficient when textured and untextured surfaces are compared. The results are referred to the best experimental result, i.e. the 150 × 600 μm elliptical geometry, with a 5% density and a 78 μm depth. A significant decrease in friction is observed for different SRRs, which becomes more marked as the average velocity drops, i.e. as the contact reaches a boundary/mixed lubrication regime. The texturing designs which can contribute to maximising this reduction are analysed in the Optimising the Designs by Means of Artificial Neural Networks section.

As it was observed in the case of circular textures,[28] wear marks were found on the discs after the tests, which is indicative of operation in areas of boundary/mixed lubrication. Figure 12 shows a contact footprint, the width of the contact mark being of the expected order of magnitude for a Hertzian contact under 20 N load, i.e. 240 μm. An increase of the contact width can be observed around the dimple, which leads to a reduction in the contact pressure. Pressure drops in a piezoviscous regime are accompanied by decreases in viscosity, which when combined cause increases in film thickness and reductions of the friction coefficient.[30] This effect contributes to delay the appearance of mixed and boundary lubrication regimes. Likewise, Figure 12 shows pits in texture outlet, which can be the result of the sudden film thickness drop at the outlet, as reported in reference[31].

OPTIMISING THE DESIGNS BY MEANS OF ARTIFICIAL NEURAL NETWORKS

Network training using experimental results

From the experimentally obtained information, a search for a texturing design that optimally combines the analysed characteristics for minimising friction was performed. To this end, an artificial neural network (ANN) was developed as information processing system.

Artificial neural networks (ANNs) are simplifications of biological neural networks which try, like the latter, to learn from input data to provide the right output.[32] They enable highly complex or

DOI: 10.1002/ls

Table IV. Friction coefficient as a function of u_m and SRR: comparison of untextured and textured results at 20 N.

u_m (mm s^{-1})	SRR = 20%			SRR = 50%			SRR = 100%			Average reduction
	Untextured	Textured	Reduction	Untextured	Textured	Reduction (%)	Untextured	Textured	Reduction	
3500	0.0145	0.0130	10%	0.0218	0.0202	8%	0.0253	0.0243	4%	7%
3000	0.0144	0.0132	8%	0.0223	0.0202	9%	0.0260	0.0246	6%	8%
2500	0.0143	0.0125	13%	0.0225	0.0197	12%	0.0271	0.0249	8%	11%
2000	0.0143	0.0122	15%	0.0226	0.0199	13%	0.0282	0.0257	9%	12%
1500	0.0141	0.0118	16%	0.0233	0.0201	14%	0.0291	0.0261	10%	13%
1000	0.0142	0.0116	19%	0.0238	0.0202	15%	0.0304	0.0269	12%	15%
500	0.0151	0.0117	23%	0.0252	0.0205	19%	0.0325	0.0281	13%	18%
250	0.0172	0.0125	27%	0.0279	0.0216	23%	0.0359	0.0292	19%	23%
100	0.0218	0.0154	29%	0.0339	0.0253	25%	0.0436	0.0334	23%	26%

DOI: 10.1002/ls

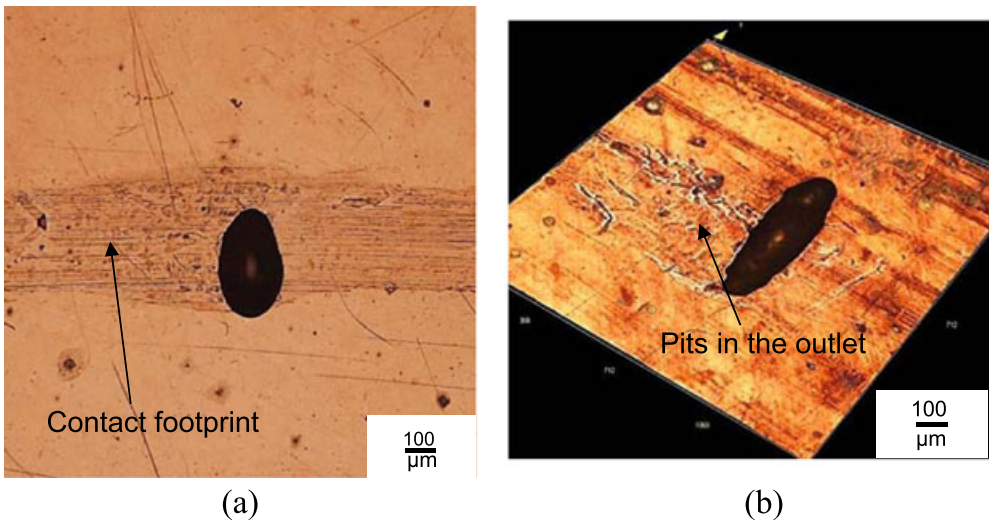

Figure 12. Surfaces of the discs after the test at 20 N. (a) Ellipses 150 × 300 μm; (b) Ellipses 150 × 600 μm. [Colour figure can be viewed at wileyonlinelibrary.com]

non-linear problems to be solved in a relatively easy manner without having to model the physical phenomena involved.[33]

Artificial neural networks (ANNs) are hierarchical and interconnected systems with elementary processing units called neurons. They may consist of one or more layers, in each of which two or more neurons are grouped together. Each neuron i of the layer j and the output k responds to an input x_m, according to Equation 6.

$$u_i^{j,k}(x_m) = f_j\left(\sum_{\forall m} W_i^{j,k} \cdot x_m + b_i^{j,k}\right) \tag{6}$$

where $W_i^{j,k}$ is a weight matrix, f_j is a transfer function and $b_i^{j,k}$ is a matrix of constants (bias matrix).

The learning process is based on providing the network with some preliminary knowledge of system responses to different inputs, which requires having many experimental results, as in our case. This training involves using the MATLAB software[34] to adjust the weight and bias matrices by means of an iterative process that compares the outputs of the network to a series of experimental data for the corresponding inputs. Then, the training is validated with a second data group that eliminates the adjustment errors introduced in the preceding phase. Finally, a final data group is used to test the overall behaviour of the ANN developed.

In this case, a simple type of ANN having a 20-neuron layer was selected, which received the input data (average velocity, SRR, load, minor and major axis dimensions, depth and texturing density) and the corresponding output (friction coefficient). The information from the MTM tests on circular geometries of previous experiments[28] and the new results for elliptical textures were used to create the ANN. It was verified that the chosen network design ensures a good balance between calculation time and accuracy.

DOI: 10.1002/ls

Once the network is trained using the described process, it can be used to predict the outputs of the system to untested input conditions. This can be applied to search for an optimal texturing design leading to the greatest reduction of the friction coefficient.[28]

Network results and optimisation possibilities

This section sets forth ANN-based simulations for quantifying the influence on friction of the surface geometry and depth of the textures. To this end, different operating conditions were considered, together with inputs in which only the design characteristics to be analysed were modified.

If the effect of depth is analysed individually (Figure 13), the created network suggests that the friction coefficient decreases as depth increases, a minimum value being obtained in the 55–65 µm range. However, the trend is reversed at greater depths.

Furthermore, the behaviours of the major and minor axes of elliptical textures were simulated separately. The size of the minor axis was simulated within an interval around the value of the Hertzian contact width. Once the minor axis is selected, the size of the major axis is determined by the eccentricity of the ellipse.

In view of the results of the network shown in Figure 14a, the size of the most favourable minor axis corresponds to a wide range of 120 to 250 µm. This circumstance leads one to question the degree of influence of this parameter, which does not seem to be a strong determining factor in the studied interval of operating conditions. In practice, this could mean an operational advantage since the textured surface would have a beneficial effect on the friction coefficient in a wide interval of operating loads.

As can be seen in Figure 14b, the results for the major axis of the ellipse predict a range of values between 400 and 700 µm, i.e. eccentricities between 1×2.5 and 1×4.5, for a maximum decrease in friction. As highlighted in the figure, elliptical patterns can lead to improvements with respect to circular patterns.

Lastly, a combined simulation of the two previous parameters was carried out: surface geometry and depth. Figure 15 shows that the most favourable results are obtained with ellipses having a ratio close to 1×4 and a depth between 50 and 80 µm.

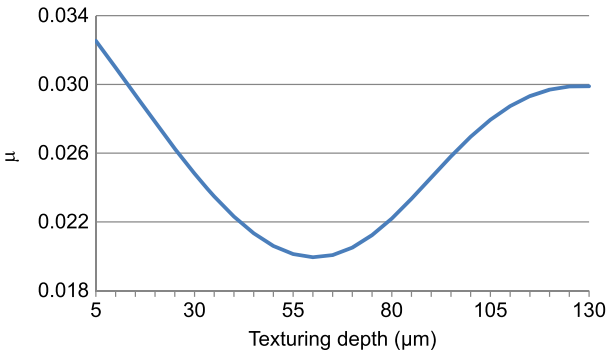

Figure 13. ANN simulation results of the effect of texturing depth in the friction coefficient. $W = 20$ N, $u_m = 300\ \text{mm s}^{-1}$, SRR = 50%, ellipses 150×600 µm and texturing density 5%. [Colour figure can be viewed at wileyonlinelibrary.com]

DOI: 10.1002/ls

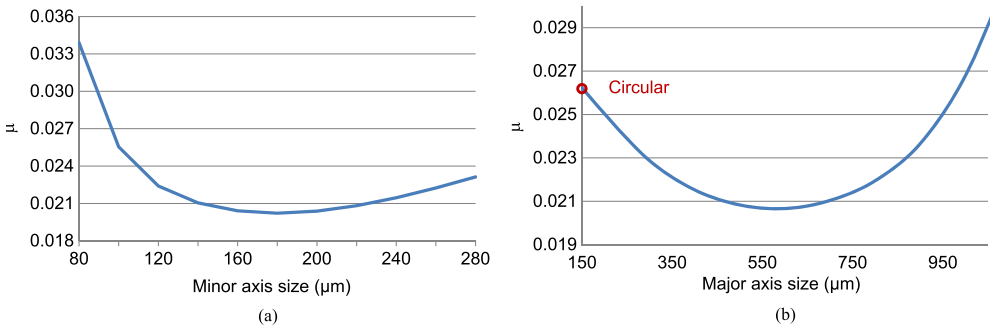

Figure 14. ANN simulation results of the effect of axes size in the friction coefficient. $W = 20$ N, $u_m = 300\,\text{mm}\,\text{s}^{-1}$, SRR = 50%, texturing density 5% and depth 78 μm. (a) Minor axis size for 600 μm major axis. (b) Major axis size for 150 μm minor axis. [Colour figure can be viewed at wileyonlinelibrary.com]

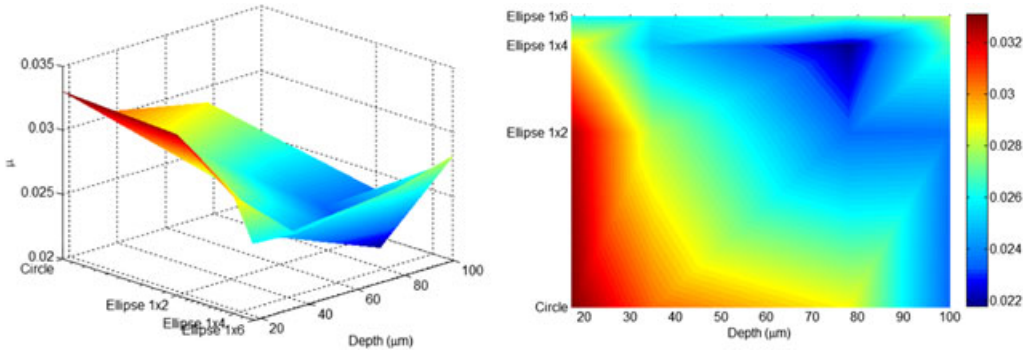

Figure 15. Optimum texturing parameters. $W = 20$ N, $u_m = 300\,\text{mm}\,\text{s}^{-1}$, SRR = 50%, texturing density 5% and minor axis 150 μm. [Colour figure can be viewed at wileyonlinelibrary.com]

Therefore, ANNs may contribute to the use of all the experimentally obtained information to predict the combination of texturing parameters that optimise the lubrication conditions, minimising the friction coefficient.

CONCLUSIONS

This paper sheds light on the benefits of texturing on the friction of lubricated contacts by means of the design and manufacture of elliptical dimples with different surface geometries, depths and texturing densities.

Each selected type was tested in a tribometer under a wide range of operating conditions, including all lubrication regimes in a ball-on-disc contact. Thus, the influence of the textures on the friction coefficient was analysed, maximum reductions being achieved in the mixed and boundary lubrication

DOI: 10.1002/ls

regimes. The benefits achieved by different combinations of major and minor axes, depths and texture densities were quantified.

Aiming at a greater decrease in friction, an ANN was developed and trained with the experiments for both the elliptical geometries analysed herein and the circular geometries studied previously. This network was used as a simulation tool, with application to the optimisation of the texturing design, showing benefits of several elliptical geometries with respect to the circular case.

One of the future challenges is to study the long-term behaviour of textured surfaces by analysing aspects such as the contact deformation and surface damage, which might affect the life of textured components.

ACKNOWLEDGEMENTS

This work was carried out as a part of the Research Project DPI2013-48348-C2-2-R, financed by the Spanish Ministry of Economy and Competitiveness. We would also like to thank the Lubricants Laboratory of Repsol.

REFERENCES

1. Hamrock BJ. Fundamentals of Fluid Film Lubrication. McGraw-Hill, New York 1994.
2. Kumar P, Khonsari MM. On the role of lubricant rheology and piezo-viscous properties in line and point contact EHL. *Tribology International* 2009; **42**(11–12):1522–1530.
3. De la Guerra E, Echávarri J, Chacón E, Munoz-Guijosa JM, Del Río B, Alén C. Analysis of the effect of different types of additives added to a low viscosity polyalphaolefin base on micropitting. *Wear* 2015; **322–323**:238–250.
4. Lainé E, Olver AV, Beveridge TA. Effect of lubricants on micropitting and wear. *Tribology International* 2008; **41**:1049–1055.
5. Bair S. Tribology and Interface Engineering Series 54, in High Pressure Rheology for Quantitative Elastohydrodynamics. Elsevier, Amsterdam 2007.
6. De la Guerra E, Echávarri J, Sánchez A, Chacón E. Film thickness predictions for line contact using a new Reynolds–Carreau equation. *Tribology International* 2015; **82**:133–141.
7. Choo JW, Olver AV, Spikes HA, Dumont MEL, Ioannides E. The influence of longitudinal roughness in thin-film, mixed elastohydrodynamic lubrication, in 60th Annual Meeting of the Society of Tribologists and Lubrication Engineers. Taylor & Francis Inc 2006: 248–259.
8. Svahn F, Kassman-Rudolphi A, Wallén E. The influence of surface roughness on friction and wear of machine element coatings. *Wear* 2003; **254**:1092–1098.
9. Habchi W. Influence of thermo-mechanical properties of coatings on friction in elastohydrodynamic lubricated contacts. *Tribology International* 2015; **90**:113–122.
10. Minami I, He X, Prakash B. Coating-lubricant combination for improving tribo-system performance. *Lubrication Science* 2014; **26**(5):375–386.
11. Hao L, Meng Y, Chen C. Experimental investigation on effects of surface texturing on lubrication of initial line contacts. *Lubrication Science* 2014; **26**:363–373.
12. Hsu SM. Surface texturing: principles and design. Maryland, USA: National Institute of Standards & Technology; November 6, 2006.
13. Pettersson U, Jacobson S. Influence of surface texture on boundary lubricated sliding contacts. *Tribology International* 2003; **36**:857–864.
14. Bhushan B. Introduction to Tribology. John Wiley & Sons, USA 2002.
15. Pirro DM, Wessol AA. Lubrication Fundamentals. Marcel Dekker Inc., New York and Basel 2001.
16. Yu H, Wang X, Zhou F. Geometric shape effects of surface texture on the generation of hydrodynamic pressure between conformal contacting surfaces. *Tribology Letters* 2009; **37**:123–130.
17. Hsu S. Integrated surface modification technology development. Presented at Oak Ridge National Laboratory on 9/15/2005.
18. Predescu A, Pascovici MD, Cicone T, Popescu CS, Grigoriu C, Dragulinescu D. Friction evaluation of lubricated laser-textured surfaces. *Lubrication Science* 2010; **22**:431–442.

DOI: 10.1002/ls

19. Wakuda M, Yamauchi Y, Kanzaki S, Yasuda Y. Effect of surface texturing on friction reduction between ceramic and steel materials under lubricated sliding contact. *Wear* 2002; **254**:356–363.
20. Nakano M, Korenaga A, Korenaga A, Miyake K, Murakami T, Ando Y, Usami H, Sasaki S. Applying micro-texture to cast iron surfaces to reduce the friction coefficient under lubricated conditions. *Tribology Letters* 2007; **28**(2):131–137.
21. Wang X, Kato K. Improving the anti-seizure ability of SiC seal in water with RIE texturing. *Tribology Letters* 2002; **14**(4):275–280.
22. Wang X, Kato K, Adachi K, Aizawa K. Loads carrying capacity map for the surface texture design of SiC thrust bearing sliding in water. *Tribology International* 2002; **36**(3):189–197.
23. Wang QJ, Zhu D. Virtual texturing: modeling the performance of lubricated contacts of engineered surfaces. *Journal of Tribology* 2005; **127**(4):722–728.
24. Lu X, Khonsari MM. An experimental investigation of dimple effect on the Stribeck curve of journal bearings. *Tribology Letters* 2007; **27**:169–176.
25. Higuera A, Gonzalez R, Cadenas M, Hernandez A. Tribological behavior of laser-textured NiCrBSi coatings. *Wear* 2011; **271**:925–933.
26. Coblas DG, Fatu A, Maoui A, Hajjam M. Manufacturing textured surfaces: state of art and recent developments. *Proc. IMechE Part J: J Engineering Tribology* 2015; **229**(1):3–29.
27. Etsion I. State of the art in laser surface texturing. *Journal of Tribology* 2005; **127**(1):248–253.
28. De la Guerra E, Echávarri J, Chacón E, Lafont P, Díaz A, Munoz-Guijosa JM, Muñoz JL. Optimising lubricated friction coefficient by surface texturing. *Proc. IMechE Part C: J. Mechanical Engineering Science* 2013; **227**(11):2610–2619.
29. Stachowiak GW. Batchelor AW. Engineering Tribology, Elsevier Butterworth-Heinemann 2005.
30. Lafont P, Echávarri J, Sánchez-Peñuela JB, Muñoz JL, Díaz A, Munoz-Guijosa JM, Lorenzo H, Leal P, Muñoz J. Models for predicting friction coefficient and parameters with influence in elastohydrodynamic lubrication. *Proc. IMechE Part J: J Engineering Tribology* 2009; **223**(7):949–958.
31. Křupka I, Hartl M. The effect of surface texturing on thin EHD lubrication films. *Tribology International* 2007; **40**(7):1100–1110.
32. Hong L, Cai J. The application guide of mixed programming between MATLAB and other programming languages, *2nd International Conference on Computer and Automation Engineering (ICCAE* 2010*)*, Singapore, pp. 185–189.
33. Echávarri J, De la Guerra E, Chacón E, Lafont P, Díaz A, Munoz-Guijosa JM, Munoz JL. Artificial neural network approach to predict the lubricated friction coefficient. *Lubrication Science* 2014; **26**(3):141–162.
34. Demuth H, Beale M, Hagan M. Neural Network Toolbox 6. User's Guides, MathWorks Inc 2010.

DOI: 10.1002/ls